Nuclear Instruments and Methods in Physics Research A 798 (2015) 135–139

Contents lists available at ScienceDirect

Nuclear Instruments and Methods in Physics Research A

journal homepage: www.elsevier.com/locate/nima

Monitoring the distribution of prompt gamma rays in boron neutron capture therapy using a multiple-scattering Compton camera: A Monte Carlo simulation study

Taewoong Lee, Hyounggun Lee, Wonho Lee *

Department of Bio-Convergence Engineering, Korea University, Seoul 136-103, Republic of Korea

ARTICLE INFO

Article history:
Received 8 July 2015
Accepted 18 July 2015
Available online 29 July 2015

Keywords:
Multiple scattering Compton camera (MSCC)
Boron neutron capture therapy (BNCT)
Born uptake regions (BURs)
Prompt gamma-ray

ABSTRACT

This study evaluated the use of Compton imaging technology to monitor prompt gamma rays emitted by ^{10}B in boron neutron capture therapy (BNCT) applied to a computerized human phantom. The Monte Carlo method, including particle-tracking techniques, was used for simulation. The distribution of prompt gamma rays emitted by the phantom during irradiation with neutron beams is closely associated with the distribution of the boron in the phantom. Maximum likelihood expectation maximization (MLEM) method was applied to the information obtained from the detected prompt gamma rays to reconstruct the distribution of the tumor including the boron uptake regions (BURs). The reconstructed Compton images of the prompt gamma rays were combined with the cross-sectional images of the human phantom. Quantitative analysis of the intensity curves showed that all combined images matched the predetermined conditions of the simulation. The tumors including the BURs were distinguishable if they were more than 2 cm apart.

1. Introduction

Boron neutron capture therapy (BNCT) is radiation therapy that entails the reaction of a stable-nucleus boron (^{10}B) and a thermal [1–3] or epithermal neutrons (1 eV to10 keV) [4–7]. Lithium (^{7}Li), an alpha particle, and a 478-keV prompt gamma ray are the products of the nuclear reaction, [8–10] i.e., $^{10}B(n,\alpha)^{7}Li$. The cross section of ^{10}B for absorbing neutrons is significantly greater than those of the elements in the human body that would surround ^{10}B. To treat a malignant tumor in the head of a patient, it is necessary to verify that a sufficient amount of ^{10}B has accumulated in the tumor to maximize the absorption of the dose of neutrons. Since the intensity of the prompt gamma rays emitted by the patient or the phantom during neutron irradiation correlates with the amount of ^{10}B present, the location of the interaction between ^{10}B and the neutron can be estimated by measuring the prompt gamma rays. Prompt gamma rays can be imaged using conventional imaging systems such as a gamma camera or single photon emission computed tomography (SPECT) [11–16]. Compton imaging technology, which uses semiconductors with 3D position-sensing techniques, has high-energy resolution and is efficient at detecting high-energy radiation (>400 keV) [17,18]. Therefore, the Compton camera can be used to detect prompt gamma rays to localize ^{10}B after neutron interaction. In addition, the combination of the reconstructed Compton images and the cross-sectional information of the phantom can accurately show the distribution of the boron uptake regions (BURs) combined with the anatomical information of the phantom.

In this study, the performance of a multiple-scattering Compton camera (MSCC), based on a thallium bromide (TlBr) semiconductor and used to monitor the three directional distribution of the tumor including the BURs in BNCT, was simulated using the Monte Carlo N-Particle eXtended (MCNPX) [19] program and quantitatively evaluated. To obtain the precise distribution of BURs in realistic conditions, we used an Oak Ridge National Laboratory (ORNL) human phantom [20]. We obtained cross-sectional images of the phantom and combined them with the reconstructed Compton images of the prompt gamma rays from the nuclear reaction of the neutrons with ^{10}B. The combined three directions images provide the precise locations of the tumor including BURs.

2. Design and method

To detect the prompt gamma rays emitted by the nuclear reaction, the MSCC detection system was positioned orthogonal to the phantom to prevent direct interaction with the neutron beam, as shown in Fig. 1. Since neutrons scattered from the patient can interfere signals of gamma ray interaction in the detectors, TlBr was chosen as the

* Corresponding author.
E-mail address: wonhol@korea.ac.kr (W. Lee).

http://dx.doi.org/10.1016/j.nima.2015.07.038
0168-9002/

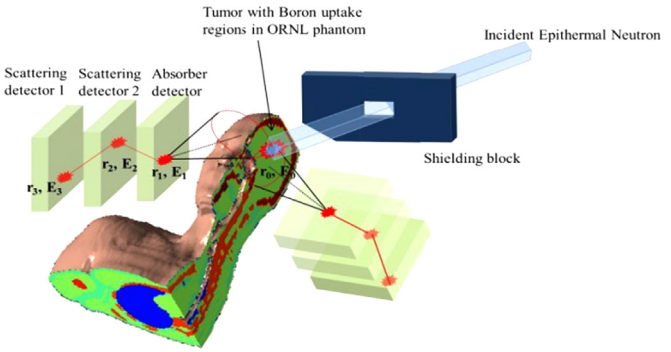

Fig. 1. Schematic diagram of the MSCC detection system for simulation.

Table 1
Absorption cross-sections for neutron (barn) of elements.

Nuclide	Neutron cross-section values (barn)	Nuclide	Neutron cross-section values (barn)
Tl	3.43	Cd	2520
Ge	2.2	Hg	372.3
Si	0.171	La	8.97

material of semiconductor detector due to their relatively low absorption cross-section for neutrons (cf. Table 1) [21]. TlBr is a promising material for medical purpose because its usability in room temperature detectors without heavy cooling devices.

The ORNL phantom used in our study was composed of more than 40 discrete cells [20]. The tumor including the BURs was inserted in the brain of the ORNL phantom and their location was checked by MCNPX visual editor. The spherical tumor with 4 cm diameter was inserted in the center of brain. The main composition and density of the tumor are same with those of the normal tissue. Boron concentrations in normal tissues and tumor volume were assumed to be 10 and 30 μg/g, respectively [22]. For realistic visualization of the cross-sectional images of phantom, we simulated a computationally coded Computed Tomography (CT) system. The source was 100 kVp X-ray fan beam and the distance between the source and the phantom was 64.5 cm. The distance between the phantom and the detector was 53.8 cm. Both source and detector of the CT were rotated 360° with 1° increments. The distance between the neutron beam source and the center of the tumor including BURs was set to 30 cm. The size and angular distributions of neutron beam were matched with size of the tumor with 4 cm diameter. The neutron flux was 1.0×10^9 n/cm^2 s, which is the minimum required for successful BNCT treatment in real-life circumstances [6,7]. The energy spectrum of the neutrons was selected based on the idealized standard reactor neutron field (ISRNF), which was calculated by Blue and Yanch [6] using the dose distribution in an accelerator-based BNCT. Assuming a tolerance dose in normal tissue, the treatment time was set to 15 min [7] for the ISRNF beam and the fluency of incident neutron in simulation models was 9.0×10^{11} n/cm^2.

To acquire the energy spectrum from the nuclear reaction in phantom, we calculated the pulse height distribution (F8 tally) including Gaussian energy broadening (GEB) function in the MCNPX code [19]. The full width at half maximum (FWHM) was determined based on the measured energy resolution of TlBr [23]. The simulated spectra show a high gamma-ray background whose main energy peaks were 511-keV and 2200-keV as shown in Fig. 2. The energy peaks represented the prompt gamma-ray emitted from pair annihilation and neutron captures in ^{1}H of the phantom. The ^{10}B neutron capture 478-keV peak was relatively small compared to the 511-keV and 2200-keV. To reduce background events such as an annihilation peak, an energy window around a 478-keV peak was applied.

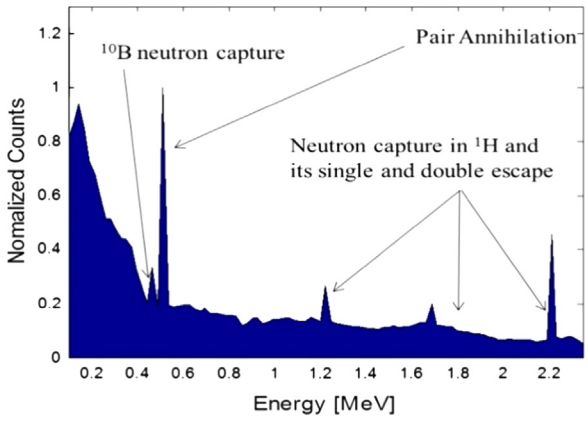

Fig. 2. Calculated prompt gamma-ray spectra after neutron captures using MCNPX code.

3. Simulation results

3.1. Geometrical optimization

The MSCC detection system consisted of three TlBr arrays to detect scattering and absorption. Each array was 40×40 pixels and $1 \times 1 \times 10$ mm^3. As shown in Fig. 3, the design parameters of MSCC detection system, such as the thickness (1 cm) of detectors for specific material and the distance between detectors (3 cm), were optimized by using Figure Of Merit (FOM) considering currently available size [24,25]. The distance between the phantom and the first scattering detector was set to 11 cm to maximize the efficiency of detecting the prompt gamma-rays. If the prompt gamma rays undergo two effective Compton scatterings followed by absorption, as shown in Fig. 1, the position (r_1, r_2, and r_3) and energy (E_1, E_2, and E_3) of each interaction is acquired by the three detectors, respectively. The incidence angle (r_0 and E_0) of the prompt gamma rays can be estimated using Compton's formula [26], and, hence, the distribution of the tumor including the BURs in the phantom can be deduced from the distribution of the prompt gamma rays. All Compton scattering data were captured in a particle-tracking PTRAC file in MCNPX code [19]. We used the maximum likelihood expectation maximization (MLEM) method, designed by Lange and Carson [27–29], to reconstruct the Compton images of the prompt gamma rays.

3.2. Reconstructed image and evaluation of performance

After discriminated by the energy window, Compton images were reconstructed based on the events of the 478-keV and 2200-keV peaks. As shown in Fig. 4, the Compton image based on the radiation from ^{10}B was clearly reconstructed as a sphere. In addition, Compton image of ^{1}H shows the tracks of the neutron beam in the phantom since hydrogen is one of wide-spread components in brain.

Fig. 5(a) shows the reference images of the simulated ORNL phantom, including the single tumor. Fig. 5(b) presents the combined images of reconstructed Compton events and the cross-sectional views of the phantom. The size of each image pixel was 2 mm. The distribution of the prompt gamma-rays represents the distribution of the tumor including the BURs in the phantom. As expected, the reconstructed Compton images were able to distinguish the tumor from the brain tissues, which enabled precise monitoring of distribution of the tumor including the BURs.

We used the intensity curves, which represent the cross-sectional distribution of the prompt gamma rays in the reconstructed Compton images, to evaluate the correlation between the prompt gamma rays and the inserted tumor including the BURs. The intensity curves seen in Fig. 6 represent the intensities of the prompt gamma rays in the